About Tree Height Measurement: Theoretical and Practical Issues for Uncertainty Quantification and Mapping

Samuele De Petris * , **Filippo Sarvia** and **Enrico Borgogno-Mondino**

Department of Agriculture, Forest and Food Sciences, University of Torino, L.go Braccini 2, 10095 Grugliasco, Italy; filippo.sarvia@unito.it (F.S.); enrico.borgogno@unito.it (E.B.-M.)
* Correspondence: samuele.depetris@unito.it

Abstract: Forest height is a fundamental parameter in forestry. Tree height is widely used to assess a site's productivity both in forest ecology research and forest management. Thus, a precise height measure represents a necessary step for the estimation of carbon storage at the local, national, and global scales. In this context, error in height measurement necessarily affects the accuracy of related estimates. Ordinarily, forest height is surveyed by ground sampling adopting hypsometers. The latter suffers from many errors mainly related to the correct tree apex identification (not always well visible in dense stands) and to the measurement process itself. In this work, a statistically based operative method for estimating height measurement uncertainty (σ_H) was proposed using the variance propagation law. Some simulations were performed involving several combinations of terrain slope, tree height, and survey distances by modelling the σ_H behaviour and its sensitivity to such parameters. Results proved that σ_H could vary between 0.5 m and up to 20 m (worst case). Sensitivity analysis shows that terrain slopes and distance poorly affect σ_H, while angles are the main drivers of height uncertainty. Finally, to give a practical example of such deductions, tree height uncertainty was mapped at the global scale using Google Earth Engine and summarized per forest biomes. Results proved that tropical biomes have higher uncertainty (from 1 m to 4 m) while shrublands and tundra have the lowest (under 1 m).

Keywords: tree height uncertainty; hypsometer; forest biomes; variance propagation law; Google Earth Engine

1. Introduction

Tree height (*H*) is a fundamental measure in forestry. It is strictly related to above-ground biomass [1,2] and canopy vertical structure [3–5]. *H* is also the most used parameter to assess a site's productivity, not only in forest ecology research, but also in forest management [6–8]. In fact, it is often used to define forest cover [9], and to assess timber quality [10] and forest ecosystem services such as forest protection against natural hazard [11] or biodiversity [12,13]. Moreover, it can be a good proxy of forest status and it is helpful in forecasting stand development and succession [14].

Nowadays, forests have a crucial role in greenhouse gas sequestration [15] and in carbon market [16], highlighting the need of accurate tree measuring. For example, for forest inventories purposes, height measurement is the most important factor, along with diameter at breast height, in estimating stand volume [17–19]. Thus, a precise forest volume computation represents a necessary step for the estimation of carbon storage at the local, national, and global scales. In this context, error in height measurement necessarily affects the accuracy of related estimates. Moreover, tree heights surveyed at the ground are usually assumed as reference data to evaluate the accuracy of the remote deductions like the ones derived by geomatics techniques such as: satellite remote sensing, light detection and ranging (LiDAR) and photogrammetry [20–22].

Ordinarily, forest height is surveyed by ground sampling adopting hypsometers [23]. The latter are lightweight instruments that can perform angular and distance measurements from which, by applying trigonometric principles, tree height is computed [24,25]. This method suffers from many errors mainly related to the correct tree apex identification (not always well visible in dense stands) and to the measurement process itself [26]. For operative reasons, in fact, hypsometric measurement is carried out without fixed supports. The hand motion during treetop/bottom collimation affects the accuracy of the angular measurement and consequently the height one [26]. In addition, operational conditions such as measuring distances, terrain slope, stem curvature, and crown shape can further affect the hypsometric measurements, introducing errors hard to detect and fix. Nevertheless, hypsometers constitute the standard instrument for dendrometric surveys, especially for forest and urban inventory purposes [27,28].

In this framework, tree height uncertainty is not ordinarily considered by users, raising some doubts about the accuracy of related forest estimates [29]. A quantification of the potential uncertainty of tree height is, therefore, essential to assess the reliability of deductions alerting the user about the significance of differences that one could test between forest stands (or single tree) or between the same stand at different times. The uncertainty knowledge is desirable especially if tree height is adopted as reference data to estimate timber volume, above-ground biomass, or carbon sink in the plant. Unfortunately, literature about the accuracy of tree height estimates by hypsometer is very limited. Although many works compared tree height derived by different instruments [6,30–33], no work can be currently found in literature about how hypsometer-based procedure affects the final estimates. In fact, for a great number of applications, there is no possibility to obtain low-cost validations concerning tree heights. This could be probably due to the fact that while measuring tree height no reference data exists for a-posteriori validation, that can be only achieved by comparing more instruments suppose showing higher accuracy. Unfortunately, this procedure requires that height survey is made contemporarily using different instruments or by cutting the tree or climbing by expensive experimental campaigns. Literature is not so exhaustive concerning this issue [26,34,35]. However, no specific work can be found concerning a comprehensive study of theoretical uncertainty affecting tree height by indirect measurements (such as the ones obtained by hypsometers). A validation based on reference datasets would be required, e.g., for very accurate and reliable measurements, the use of height poles/sticks with climbing is mostly used method by researchers and arborists [32,36]. Although this was possible (albeit expensive) for research purposes, it would be no longer applicable for operative purposes. The only alternative is therefore to model the expected theoretical uncertainty.

In the proposed study, a statistically based operative method for estimating height measurement uncertainty was proposed using the variance propagation law (VPL) [37]. VPL uses the accuracies of direct measurements (in this work, angles and distances), assumed to be known, to estimate the theoretical variance of the indirect measurement (in this work, the tree height). Some simulations were performed involving several combinations of terrain slope, tree height, and distances by modelling the behaviour of height uncertainty and its sensitivity to such parameters. The results have been summarized in graphs that constitute an operational tool giving an estimate of the uncertainty of tree height and assess its goodness compared to the expected application avoiding tree cut or climbing on. Finally, to give a practical example of such deductions, tree height uncertainty was mapped at the global scale using Google Earth Engine (GEE) and summarized per forest biomes.

2. Materials and Methods

The workflow adopted in this work is reported in Figure 1. Using field surveys, the angular error of hypsometer was modelled. Subsequently, tree height uncertainty was modelled by VPL, and a sensitivity analysis of this model was performed. Some theoretical scenarios were given to explore tree uncertainty behaviour under different environmental and operative conditions. Finally, to give a practical interpretation of theoretical deductions,

using Google Earth Engine (GEE) platform, the height uncertainty at the global scale was mapped and summarized according to forest biomes.
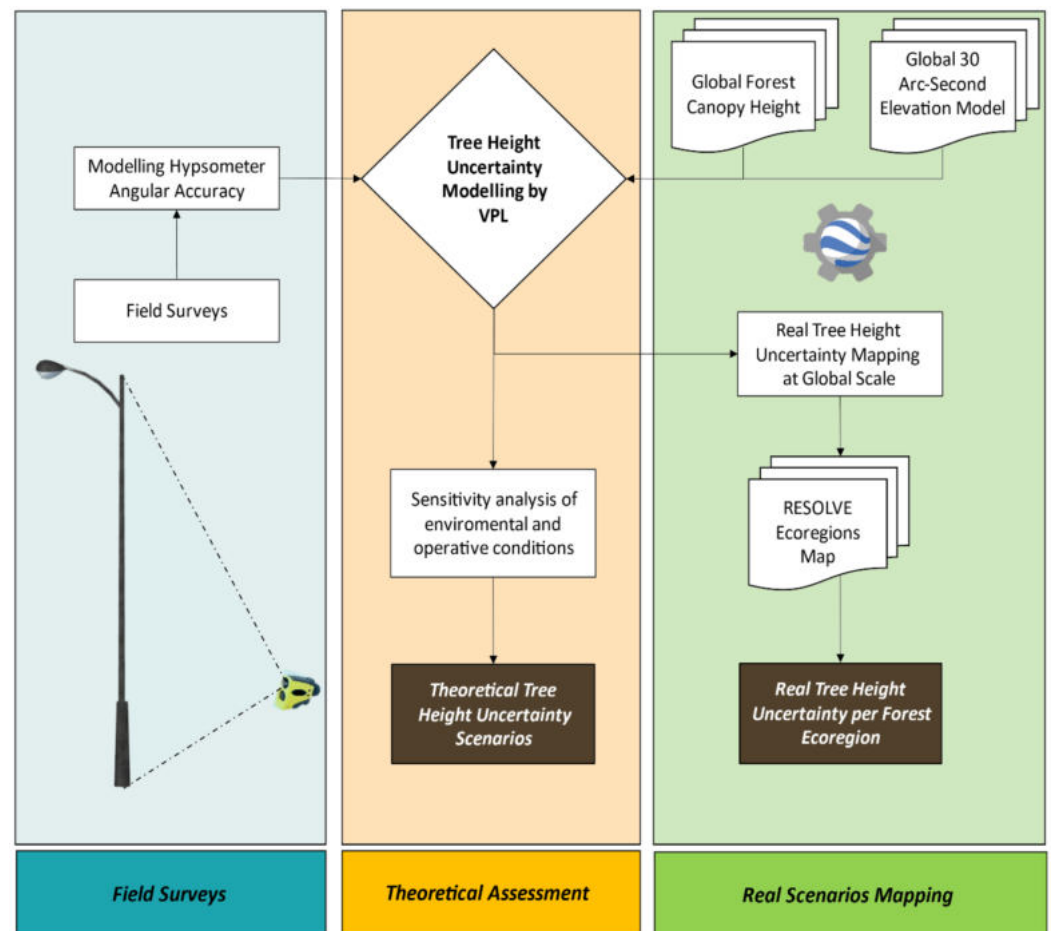
Figure 1. Workflow adopted. Starting from field surveys, the hypsometer accuracy was modelled. Theoretical evaluations were performed concerning the formalization of tree height uncertainty model. Subsequently, a sensitivity analysis and theoretical scenarios were provided. Finally, globally available data in GEE was used to explore real tree height uncertainty for each forest ecoregion.

2.1. Available Data

2.1.1. Experimental Design of Field Surveys

Hypsometric measures are ordinarily performed with no fixed support thus introducing a variability due to the operator's hand motion in collimation that affects angle measures. The controlled laboratory environment provided an important test for bias, but could not provide a realistic evaluation of instrument performance under field conditions [6]. The latter is affected by three kinds of uncertainty: instrumental, environmental, and operative uncertainty. The first one is related to instrumental feature/quality and can be estimated in laboratory. The second one is related to environmental conditions such as: terrain slope, air moisture, temperature, tree apex visibility, tree stem shape, and inclination. Unfortunately, these conditions cannot be directly controlled by the user during the survey. Otherwise, operative conditions such as slant range (*SR*) between tree and instrument can be managed by the operator and properly set to optimize final accuracy. Nevertheless, due to terrain asperity or cost/time-related limitations, operative conditions are often not properly considered and addressed. All these issues deeply affect the angular measures of hypsometer, reflecting into not neglectable errors in tree height computation. Currently, very few works about angular accuracy of forest hypsometers are present in literature. Trying to fill this lack, in this work, a reference light pole was used to test the precision of

the hypsometer angle measures under operative conditions. The choice of adopting a static and invariant object such as a light pole moves deductions from a particular context to general one. This is mainly related to the well-known and objective operational difficulty of selecting the proper apex of a tree (especially from different users). For this reason, we repeated our experiment with reference to a pole located in a flat and open area. It is worth to remind that repetition from different users was differently aimed at providing a more robust estimate of actual instrument uncertainty, completing the one supplied by producer with the one related to the user (that has to be intended as part of the instrument). It is obvious that provided estimates will be "optimistic" since, operationally speaking, one has, for example, to consider that the apex of the tree is not so unique to be defined as the apex of a pole.

A light pole, having a height of 15 m, placed in the Campus of Department of Agriculture, Forest and Food Sciences of Torino University (NW Italy, 45° 3′55.38″ N–7°35′30.61″ E) was selected. It is isolated and therefore its apex well visible from the ground. The pole is not inclined and terrain slope around is lower than 5°. The TruPulse 200/B laser rangefinder was used. It operates through a laser (near infrared pulse) coupled to a tilt sensor. TruPulse has nominal slant range accuracy (σ_{SR}) equal to 1 m and angular accuracy (σ_{ang}) equal to 0.25° [38]. Before the survey, tilt sensor was calibrated according to manual requirements.

Four expert operators performed pole height surveys according to the follows experimental design (Figure 2). Angle measures (respectively pointing at pole top and pole bottom) were surveyed three times per operator moving around the pole along 3 geographical directions (N, SW, and SE) placed at 120° to each other. For each direction, *SR* changes from 10 m to 40 m with 10 m steps. It is worth to highlight that additional measurements were operated by positioning the instrument in an open field and pointing the laser of the TruPulse towards a reflecting signal placed close to the pole (at 1.6 m from ground) in order to measure and compensate for the terrain slope contribution. Then, angles collimating top (θ) and bottom (α) were surveyed. A total of 144 height surveys and 288 angle measures were performed over the same pole.
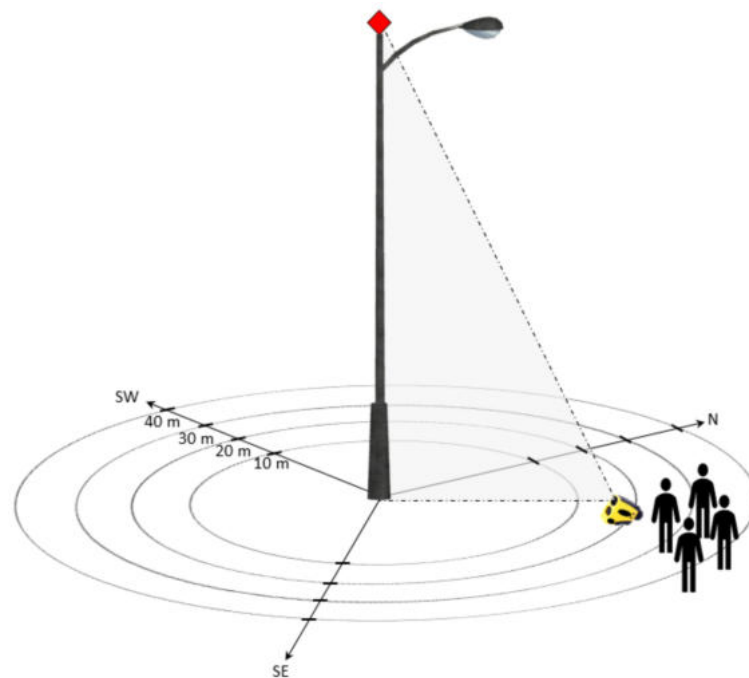
Figure 2. Experimental design adopted in this work involving four operators. Three geographical direction placed at 120° apart were used pointing to the: North, South-East, and South-West. For each position, 3 replicas were measured. Red rhombus is the pole top collimated during the height survey placed at 10 m, 20 m, 30 m, and 40 m distance, respectively.

2.1.2. Geographical Data

The Global Forest Canopy Height (GFCH) represents global tree heights based on a fusion of spaceborne-lidar data from the Geoscience Laser Altimeter System (GLAS) and ancillary geospatial data [39]. GFCH is provided in GEE as raster layer having a geometric resolution of 1 km and updated in 2005. The accuracy in forest height estimation ranges between 3.8 m and 6 m according to forest types [39,40].

The Global 30 Arc-Second Elevation (GTOPO30) is a global digital elevation model (DEM) with geometric resolution of about 1 km. The DEM was derived from several raster and vector sources of topographic information and was updated in 1996 [41]. Currently, it represents the only available DEM in GEE covering the entire globe including high latitude zones (i.e., Boreal, Artic and Antarctic zones).

In order to explore and summarize tree height uncertainty over the world, the RESOLVE Ecoregions map (REM) was adopted in GEE. REM is a vector layer representing about 476 forested ecoregions grouped in 14 forests biomes. It was updated in 2017 and is the most update dataset on remaining habitat in each terrestrial ecoregion [42]. Table 1 reports the REM biomes and the code adopted in this work.

Table 1. Forest biomes present in the RESOLVE Ecoregions map.

Biomes	Code (ID)
Tropical and Subtropical Moist broadleaf Forests	B1
Montane Grassland and Shrublands	B10
Tundra	B11
Mediterranean Forests, Woodlands, and Scrub	B12
Deserts and Xeric Shrublands	B13
Mangroves	B14
Tropical and Subtropical Dry broadleaf Forests	B2
Tropical and Subtropical Coniferous Forests	B3
Temperate Broadleaf and Mixed Forests	B4
Temperate Conifer Forests	B5
Boreal Forests or Taiga	B6
Tropical and Subtropical Grassland, Savannas, and Shrublands	B7
Temperate Grassland, Savannas, and Shrublands	B8
Flooded Grassland and Savannas	B9

2.2. Data Processing

2.2.1. Uncertainty Modelling

Tree height measurement by hypsometer is effective and widely used in forestry, being the standard and reference procedure to validate measures from remote sensing. Tree height uncertainty is not ordinarily considered by users [43]; conversely, it could proficiently support deductions, especially to assess significant differences in both spatial and time domain. A quantification of the potential uncertainty of tree height is, therefore, essential to support the reliability of deductions especially if tree height is adopted as reference data to estimate wood volume, above-ground biomass, or carbon stocked. Although a precise reference value can be obtained for research purposes, it would be no longer applicable for operative purposes. The only alternative is therefore to model the expected theoretical uncertainty. The variance propagation law (VPL—Equation (1)) is the statistical tool that ordinarily can be used for this task [37]. It models the effect of variance (ordinarily assumed as indicator of squared precision) of direct measures (i.e., angular and distance measures) onto the variance of the derived measures (i.e., tree height).

$$\sigma_y^2 = \left(\frac{\partial y}{\partial x_1}\right)^2 \cdot \sigma_{x_1}^2 + \left(\frac{\partial y}{\partial x_2}\right)^2 \cdot \sigma_{x_2}^2 + \ldots + \left(\frac{\partial y}{\partial x_n}\right)^2 \cdot \sigma_{x_n}^2 + 2\sum_{i=1}^{n-1}\sum_{j=i+1}^{n}\left(\frac{\partial y}{\partial x_i}\right)\left(\frac{\partial y}{\partial x_j}\right) COV(i,j) \tag{1}$$

where $y = f(x_1, x_2, \ldots, x_n)$ is the dependent variable, x_i the independent ones, and $\sigma^2_{x_i}$ their variance (supposed known); $COV(i, j)$ is the covariance between the i-th and j-th independent variables. The starting point to successfully operate with VPL is to define the model formula it has to be applied to. Ordinarily, tree height is computed by hypsometer according to Equation (2) following the procedure summarized in Figure 3.

$$H = (SR \cdot \cos \varphi) \cdot (\tan \theta + \tan \alpha) \tag{2}$$

where SR is the slant range between tree stem and operator; φ is the terrain slope measured by pointing the reflecting pole near trunk at operator eye level (here set 1.6 m); and θ and α are the angles derived by the collimation of tree top and tree bottom, respectively.
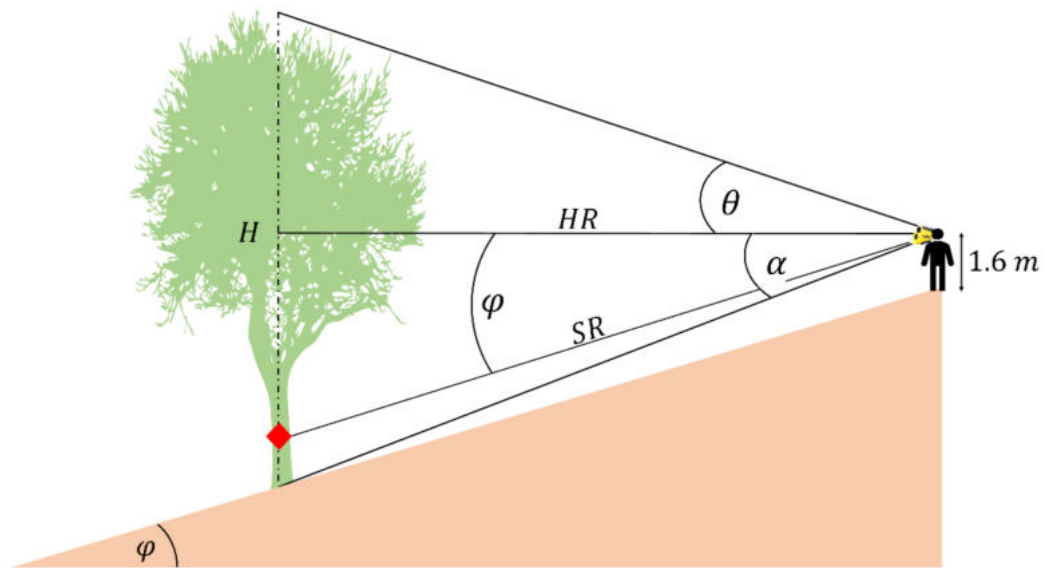
Figure 3. Reference framework involved during hypsometer survey. H is the tree height aboveground; φ is the terrain slope measured by pointing the rangefinder to the reflecting pole near the trunk (red rhomb); SR is the slant range (tree-operator distance) and HR is the horizontal distance; and θ and α are the angles measured by tilt sensor (digital clinometer) collimating tree top and tree bottom, respectively. For this work, operator height is fixed at 1.6 m.

Direct measures involved in H computation are the angles and distance measures (i.e., φ, θ, α and SR); consequently, H uncertainty (σ_H—Equation (3)) can be computed applying Equation (1) to Equation (2), considering that trigonometric relationships exist between variables.

$$\sigma_H = \sqrt{\left(\frac{\partial H}{\partial SR}\right)^2 \sigma^2_{SR} + \left(\frac{\partial H}{\partial \varphi}\right)^2 \sigma^2_{\varphi} + \left(\frac{\partial H}{\partial \alpha}\right)^2 \sigma^2_{\alpha} + \left(\frac{\partial H}{\partial \theta}\right)^2 \sigma^2_{\theta} + 2\left(\frac{\partial H}{\partial SR}\right)\left(\frac{\partial H}{\partial \alpha}\right) COV(SR, \alpha) + 2\left(\frac{\partial H}{\partial SR}\right)\left(\frac{\partial H}{\partial \theta}\right) COV(SR, \theta)} \tag{3}$$

where partial derivatives involved in Equation (3) are reported in Table 2. Precision values are σ_{SR} the uncertainty of laser rangefinder assumed equal to the nominal one (i.e., 1 m); σ_{φ}, σ_{θ}, and σ_{α} are the uncertainties of hypsometer angles. Despite the same instrument was used, angles measured are affected by different factors. For this reason, in this work, above-mentioned precision and covariance values were explored and estimated separately.

Table 2. Partial derivatives involved in Equation (3).

Partial Derivatives
$\frac{\partial H}{\partial SR} = \cos\varphi(\tan\theta + \tan\alpha)$
$\frac{\partial H}{\partial \varphi} = -(SR\ \sin\varphi)(\tan\theta + \tan\alpha)$
$\frac{\partial H}{\partial \alpha} = (SR\ \cos\varphi)\ (\tan^2\alpha + 1)$
$\frac{\partial H}{\partial \theta} = (SR\ \cos\varphi)\ (\tan^2\theta + 1)$

In fact, hypsometer angles uncertainty is affected by two main components and can be linearly modelled similarly to other topographic instruments [44,45]. The first is a constant term (intercept—β_0) related to the instrument accuracy itself and assumed equal for φ, θ, and α, while the second one is related to operator collimation accuracy (gain—β_i) mainly dependent from SR and hand stability. Since β_0 can be estimated in the laboratory, it is ordinarily provided by the producer. In this work, using TruPulse 200B, β_0 was assumed to be equal to σ_{ang}, while β_i was properly calibrated using ordinary least squares involving angular measure derived from field surveys. According to the previously mentioned experimental design, at each position, three replica were acquired and related standard deviation computed and assumed as precision of angular measure probably related to hand operator stability. Then, precision values were fitted against the SR. Finally, β_i concerning θ and α were modelled by a power model ($\beta_i = aSR^b$ and σ_θ and σ_α were computed (Equations (4) and (5)). Furthermore, the Mean Absolute Percentage Error (MAPE) was computed involving the residuals of regressions (power models part in Equations (4) and (5)). Since MAPE values are computed by removing the SR dependence from angle precision models, the remaining error component could be probably due to operator variability (i.e., hand motion and collimation accuracy). Concerning φ, it is ordinary measured without the operator collimation process but simply by pointing laser to reflecting pole. Therefore, σ_φ can be assumed equal to β_0.

$$\sigma_\theta = \beta_0 + aSR^b \tag{4}$$

$$\sigma_\alpha = \beta_0 + cSR^d \tag{5}$$

where a, b, c, and d are the model coefficients. Moreover, the covariance between θ and SR, $cov(\theta, SR)$, and covariance between α and SR, $cov(\alpha, SR)$, were computed using filed surveys involving a total of 288 angle measures.

A sensitivity analysis was then performed to explore how different variables mainly affect σ_H. Some scenarios were run varying H values from 5 m and 40 m, changing φ values from 5° to 45° and SR from 10 m to 50 m using Equation (3). Then, σ_H behaviour was explored by plotting φ and SR trends, parametrizing resulting functions by H values. A final scenario was computed using Equation (3), setting $\varphi = 15°$ and all possible combination of H and SR in σ_H computation. The analysis requires that the above-mentioned formulas are computed using the expected angular values corresponding to a certain tree height. This can be obtained once tree height, SR, operator's height, and terrain slope are known.

It is worth to note that precision values involved in Equation (3), once propagated by VPL, contribute differently to final H variance. Therefore, we measured the relative weight (importance) of each factor variance on H variance according to formula reported in Table 3 and changing SR from 5 m to 50 m.

Table 3. Relative weights affecting variance of H.

Factor	Formula
Sum of weights	$\Sigma = \left(\frac{\partial H}{\partial SR}\right)^2 + \left(\frac{\partial H}{\partial \varphi}\right)^2 + \left(\frac{\partial H}{\partial \alpha}\right)^2 + \left(\frac{\partial H}{\partial \theta}\right)^2 +$ $2\left(\frac{\partial H}{\partial SR}\right)\left(\frac{\partial H}{\partial \alpha}\right) COV(SR,\alpha) + 2\left(\frac{\partial H}{\partial SR}\right)\left(\frac{\partial H}{\partial \theta}\right) COV(SR,\theta)$
Slant Range	$w_{SR} = \frac{\left(\frac{\partial H}{\partial SR}\right)^2}{\Sigma}$
Terrain slope	$w_{\varphi} = \frac{\left(\frac{\partial H}{\partial \varphi}\right)^2}{\Sigma}$
Angle pointing tree bottom	$w_{\alpha} = \frac{\left(\frac{\partial H}{\partial \alpha}\right)^2}{\Sigma}$
Angle pointing tree apex	$w_{\theta} = \frac{\left(\frac{\partial H}{\partial \theta}\right)^2}{\Sigma}$
Mixed term considering SR and α correlation	$w_{corr(SR,\alpha)} = \frac{2\left(\frac{\partial H}{\partial SR}\right)\left(\frac{\partial H}{\partial \alpha}\right) COV(SR,\alpha)}{\Sigma}$
Mixed term considering SR and θ correlation	$w_{corr(SR,\theta)} = \frac{2\left(\frac{\partial H}{\partial SR}\right)\left(\frac{\partial H}{\partial \theta}\right) COV(SR,\theta)}{\Sigma}$

2.2.2. Mapping Tree Height Uncertainty at the Global Scale

Scenarios were run to explore σ_H theoretical behaviour and which factor mainly affects it. Despite theoretical scenarios, to give a practical example aimed at proposing an operational scenario, the above-mentioned concerns were applied at the global scale using Google Earth Engine (GEE) and developing an appropriate routine. GEE is an web-based platform that allows an immediate access to geographical data and performing wide areas analysis [46]. GEE consists of a multi-petabyte analysis-ready data catalogue and its parallel computation service allows to process large geospatial datasets at the global scale. For this reason, GEE was used in this work to map σ_H at the global level implementing Equation (3). To perform such task, the following pre-processing steps were involved. GTOPO30 layer was used to compute local terrain slope, $\varphi(x,y)$, while the GFCH was assumed a reliable dataset that provides a continuous estimate of forest height, $H(x,y)$, around the world. Involving $H(x,y)$ and $\varphi(x,y)$, Equation (3) was applied directly in GEE to estimate height uncertainty at the pixel-level. Four maps of H uncertainty, $\sigma_H(x,y)$, were computed setting SR equal to 10 m, 20 m, 30 m, and 40 m, respectively, in order to compute σ_H value one can expect if placed at given distance to the tree. Finally, REM biomes polygons were used as spatial basis to compute the 5th, 25th, 50th, 75th, and 95th percentiles of $\sigma_H(x,y)$, providing information about the density function over world forest biomes. These maps, coupled to density function, allow the operator to plan forest surveys and properly manage the tree height uncertainty during his/her surveys, alerting about the significance difference existing if comparing the height measures over time or in space.

3. Results

3.1. Uncertainty Modelling

Uncertainty of angular measures from hypsometer is related to both instrument accuracy and operator skills. The former is the one provided by the producer; the latter has to be somehow estimated. Angular accuracy of hypsometer proved to follow a power model (Equations (4) and (5)) that was opportunely calibrated by least square-based regression (Figure 4) involving θ and α values from field surveys. Model coefficients were reported in Table 4. They showed to be significantly different from 0.

(a)

(b)
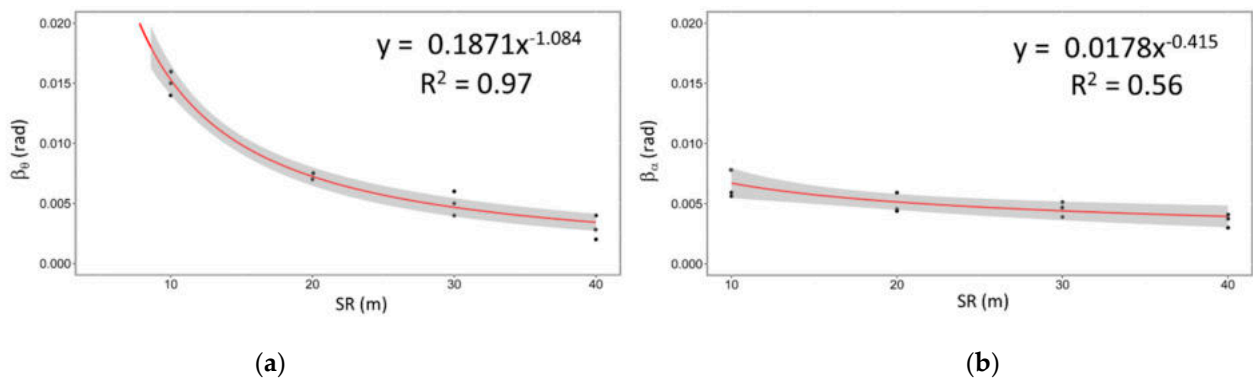
Figure 4. (a) β_θ vs. *SR* model calibrated from field data (radians values); (b) β_α vs. *SR* model calibrated from field data. Grey bounds are the 95% confidence intervals, red lines are the calibrated models.

Table 4. Hypsometer accuracy models coefficients (Equations (4) and (5)).

Coefficient	Value	Standard Error	t	p-Value
a	0.1871	0.0031	3.25	0.0051
b	−1.0841	0.0874	3.92	0.0064
c	0.0178	0.0035	3.22	0.0094
d	−0.4156	0.1232	3.65	0.0053

Figure 4a shows that, generally, β_θ decreases as *SR* increases. In particular, an increase of *SR* from 10 m to 20 m determines a β_θ reduction by half of its value, going from a value of 0.015 radians to one of 0.007 radians, respectively. Subsequently, for *SR* equal to 30 m up to 40 m, β_θ decreases by 0.002–0.003 rad, respectively. A similar behaviour can be observed in Figure 4b. However, in this case, the β_α variation appears to be milder and generally a flat behaviour characterizes β_α. Nevertheless, when *SR* is equal to 10 m, β_α is two times lower than β_θ (0.007 rad and 0.015 rad, respectively); for *SR* greater than 30 m, β_α results to be similar β_θ (0.005 rad).

Based on results, it appears that for low *SR* values, uncertainty of angular measurements results to be higher in θ than in α, whereas with high *SR* values the two uncertainties turn out to be similar. In fact, fixing tree height, if *SR* increase both θ and α angles should decrease. Therefore, for higher angles (i.e., the ones generated by treetop collimation), higher their uncertainty. Similarly, angles generated by bottom collimation follow this trend, however since they are smaller, their uncertainty results lower. Concerning this issue, Bragg [47] highlighted that moving away from the target, angles measurements can be more accurate decreasing the errors related to the tree height determination. MAPE concerning β_θ is 15%, while 14% for β_α. Since these MAPE values represent angle accuracy component not dependent from SR, both values suggest that about the 15% of the error is not due to operative condition (SR) but by operator-related ones. The latter could probably be due to higher/lower operator hand motion accuracy during the surveys, suggesting how a fixed support could improve hypsometer survey accuracy [6]. Using filed data $cov(\theta, SR)$ and $cov(\alpha, SR)$ were found equal to −0.95 and 0.27, respectively. These values suggest that θ is more correlated to *SR* than α as also proved by the determination coefficients of calibrated models ($R^2 = 0.97$ and $R^2 = 0.56$ for β_θ and β_α, respectively).

To assess the effects of angle accuracy and other operative conditions on tree height uncertainty, VPL was adopted, and some theoretical scenarios were proposed involved the hypsometer angle precision models previously calibrated. In particular, two scenarios were explored, the first one by applying VPL changing φ and parameterizing Equation (3) by H (Figure 5a). The second one was obtained by applying VPL changing *SR* and parameterizing Equation (3) by H (Figure 5b).
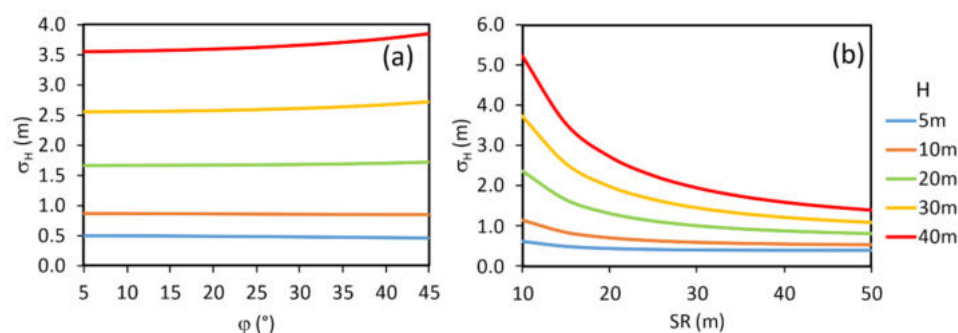
Figure 5. (**a**) σ_H scenarios derived by applying VPL changing φ and parameterizing Equation (3) by H; (**b**) σ_H scenarios derived by applying VPL changing SR and parameterizing Equation (3) by H.

Generally, Figure 5a shows that σ_H does not significantly change even if φ increases. Moreover, the σ_H value results to be very high ($\sigma_H > 3.5$ m) with H values equal to 40 m, while are lower ($\sigma_H = 0.5$ m) for H values equal to 5 m. Furthermore, it can be highlighted that with φ values greater than 35–40°, σ_H values increase slightly. For example, considering $H = 40$ m and $\varphi = 25°$, the σ_H value results to be equal to 3.5 m, while at 45° it turns out to be equal to 3.8 m, showing an increase of σ_H equal of about 9%. Consequently, it would appear that σ_H would only be affected by high levels of slope ($\varphi > 30°$). This result was supported by Stereńczak et al. [26], who found that slope, especially when height measurement is made below the tree base, can increase height errors.

Conversely, considering Figure 5b, the σ_H value appears to be strongly affected by SR. Specifically, σ_H tends to decrease as SR increases. For example, assuming H equal to 40 m, the σ_H value results to be 5 m, 3 m, 2.5 m, 2.2 m, and 1.8 m for the respective SR values of 10 m, 20 m, 30 m, 40 m, and 50 m. Whereas, if H is 5 m, σ_H remains constant around 0.80 m despite SR variations.

Considering taller trees (between 20 m and 40 m), σ_H results to be very high especially for SR low values (between 10 m and 20 m); moving away from the tree (SR between 30 m and 40 m), σ_H decreases until it stops with values of $SR > 40$ m. However, this behaviour does not appear with smaller trees ($H < 10$ m). Similar results were reported by Skovsgaard [6], who showed that higher SR positively affect the estimation of tree height.

Based on these results, it appears that the parameters H and SR significantly affect σ_H value. Therefore, by combining these two parameters, it was possible to report several σ_H scenarios that might normally occur during field surveys (Figure 6).

In particular, Figure 6 shows that σ_H values increase when H increases and SR decreases. Nevertheless, fixing H, σ_H could greatly vary depending on SR. For example, having SR and H equal to 60 m and 30 m, respectively, a σ_H can be found equal to 1 m. Otherwise, having SR and H equal to 6 m and 30 m, respectively, a σ_H can be found equal to 9 m (i.e., about one order of magnitude than $SR = 60$ m).

From an operational point of view during height survey, the proper combinations of H and SR that can be proposed based on scenarios in Figure 6. Three main operative conditions can be defined: (i) distance from the target half to the tree height ($SR = 0.5\ H$); (ii) distance from the target equal to the tree height ($SR = H$); and (iii) distance from the target twice to the tree height ($SR = 2\ H$). In the first case, having the H-SR ratio equal to 2:1, the σ_H value, and consequently the errors in tree height estimation, would increase considerably. For example, with H equal to 20 m and SR equal to 10 m, the σ_H values would be equal to 2.5 m resulting in an error range between 12.5% compared to the tree height. Concerning the second case, having the H-SR ratio equal to 1:1, for example a tree of 20 m and placed at 20 m, σ_H will be about 1.5 m, i.e., 7.5% error compared to H. Considering the ratio 1:2, the σ_H would decrease considerably. For example, with $H = 20$ m and $SR = 40$ m, σ_H values result to be equal to 0.8 m, i.e., 3.5% error compared to H. However, it is worth to remind that the last condition is not always allowed during field surveys. In fact, several works [26,48,49] proved that moving away from the target, treetop visibility can be masked

by others tree crown. Therefore, based on our results, a simple rule of thumb can be proposed: a *H-SR* ratio equal to 1:2 (environmental conditions permitting) would be the most reasonable operative choice to minimize relative tree height uncertainty under the 5%.
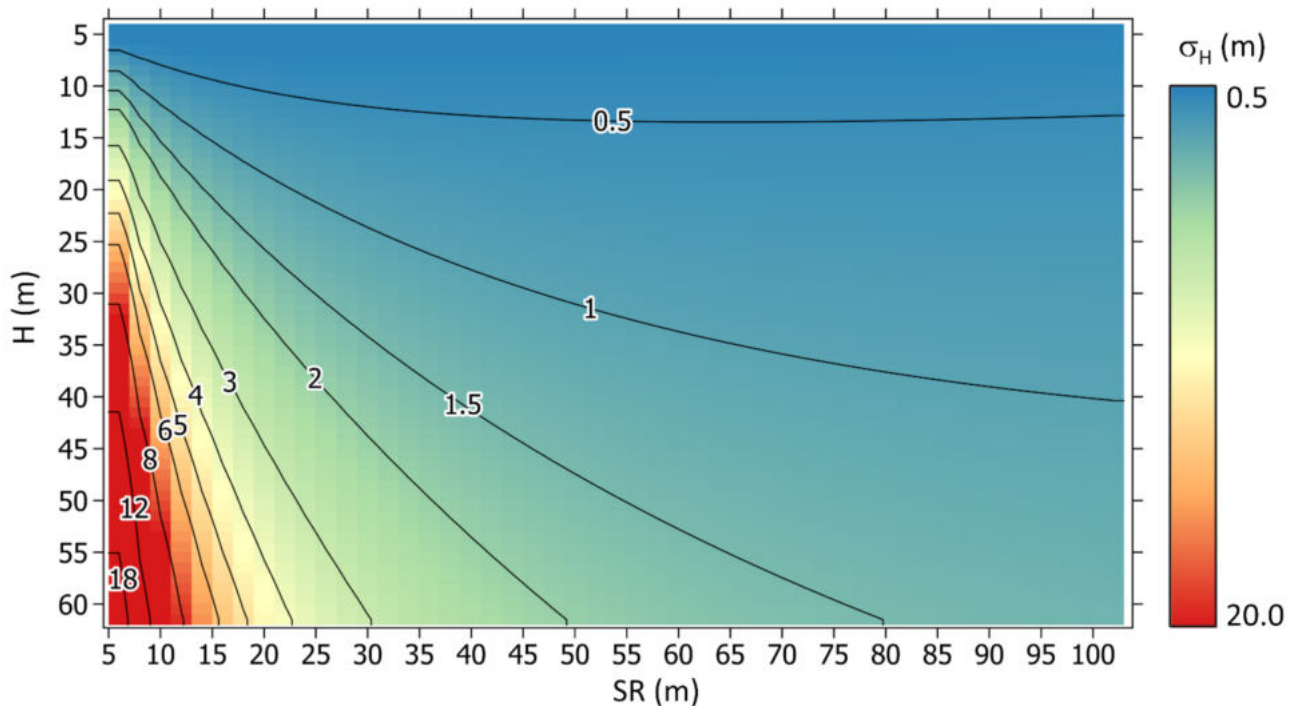
Figure 6. σ_H scenarios ($\varphi = 15°$) obtained by all possible combination between *H* and *SR*. Isolines represent line having same σ_H.

In order to better assess the effect of the different parameter uncertainty involved in σ_H computation, a sensitivity analysis of σ_H was performed. In Figure 7, the weights of tree height variance computed applying Table 3 formulas are reported.

It can be noted that, generally, the parameters that most affect $\sigma_H{}^2$ result to be w_α and w_θ. Indeed, their sum reaches about 95% of tree height variance in all scenarios. Conversely, $w_{corr (SR,\alpha)}$, $w_{corr(SR,\theta)}$, w_φ, and w_{SR} poorly affect $\sigma_H{}^2$ (under 2% on average). Concerning this issue, w_θ and w_α appear to be strongly affected by *SR* and *H*. In fact, for smaller tree (e.g., $H = 5$ m), the values of w_θ and w_α are constant as *SR* increase; for $H > 10$ m, the weight of w_α increases as *SR* increases, while w_θ decreases. Considering weights from same SR, it can be observed that w_α and w_θ significantly vary according to *H* values, while other weights remain low. In particular, at low *SR* values, w_θ tends to increase according to *H* increase. Conversely, at high *SR* values, w_θ increase little as *H* increases. For example, with *SR* equal to 10 m, w_θ result to be about 47% and 90% with *H* equal to 5 m and 40 m, respectively. Whereas with *SR* equal to 40 m, w_θ results to be again 47% with *H* equal to 5 m but about to 60% with *H* equal to 40 m. Therefore, the treetop angle (θ) uncertainty participates for the most of tree height uncertainty for $H > 5$ m. For the same *H*, increasing the *SR* value the angle θ and the corresponding w_θ in the σ_H computation decreases and, as a consequence, the w_α increases. Another interesting conclusion concerns the importance of terrain slope and *SR* accuracy. In fact, in all scenarios, the w_φ and w_{SR} are lower than 1%, suggesting that a coarse estimate of such parameters does not significantly affect tree height uncertainty. Therefore, more accurate rangefinder does not directly reflect in better tree height estimates suggesting that similar tree height accuracy can be obtained by using laser, ultrasound, or optical telemeter. Similar results were found by [6,50] where different forest rangefinder were compared.
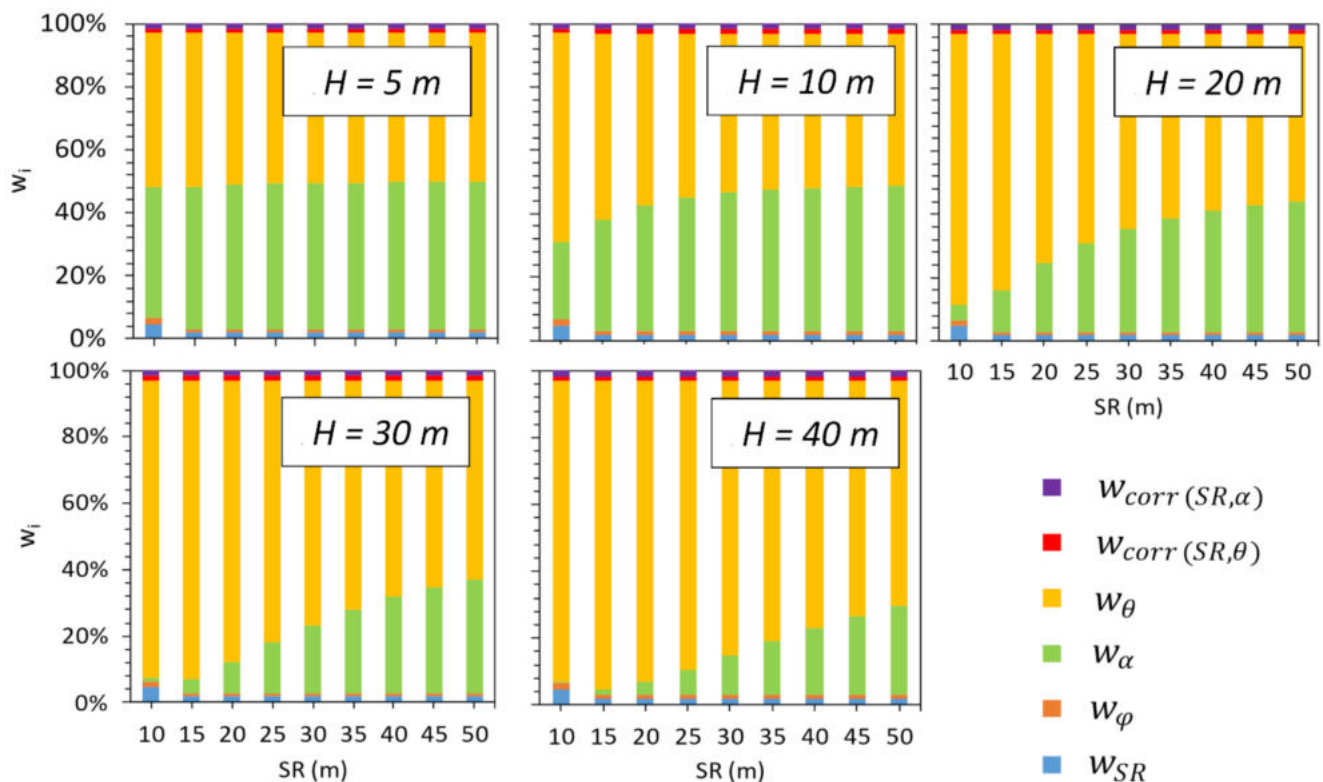
Figure 7. Relative weights (importance) of factors involved in the sensitivity analysis of $\sigma_H{}^2$. Sensitivity analysis was iteratively performed by computing w_i changing H and SR.

3.2. Mapping Forest Height Uncertainty at the Global Scale

To give a practical example of the theoretical scenarios, an appropriate GEE routine was developed in order to map tree height uncertainty at global scale. Since the distance between tree and the operator was found to greatly affect the height uncertainty, four different scenarios with SR equal to 10, 20, 30, and 40 m were proposed (Figure 8). Mapping was achieved according to the same approach used for generating the graph of Figure 6. In this case, the local tree height estimate was obtained from GFCH and the local slope value from GTOPO30; an operator's height of 1.60 m was used for all computations. It is worth to stress that GFCH was simply used to derive an estimate of local tree height in order to generate an estimate of the associated uncertainty if obtained by ground surveys operated as modelled in this work. In other words, we did not model the uncertainty of GFCH, but we used GFCH to inform users that are going to operate ground surveys in those areas about the expected theoretical accuracy of their measurements.

Generally, σ_H tends to decrease when SR increases, confirmed by the previous-mentioned role of tree-operator distance. For example, considering the Amazon zone, σ_H results to be greater than 5 m at $SR = 10$ m, while at $SR = 40$ m, σ_H result about 1.5 m, thus about 75% more accurate. It is worth to remind that a coarse DEM was involved in these simulations. Therefore, slope values are affected by this low resolution probably providing underestimated slopes especially in those areas characterized by high topographic variability (e.g., mountain).

To summarize $\sigma_H(x, y)$ differences at global level, $\sigma_H(x, y)$ percentiles per forest biomes were computed and reported in boxplots (Figure 9).
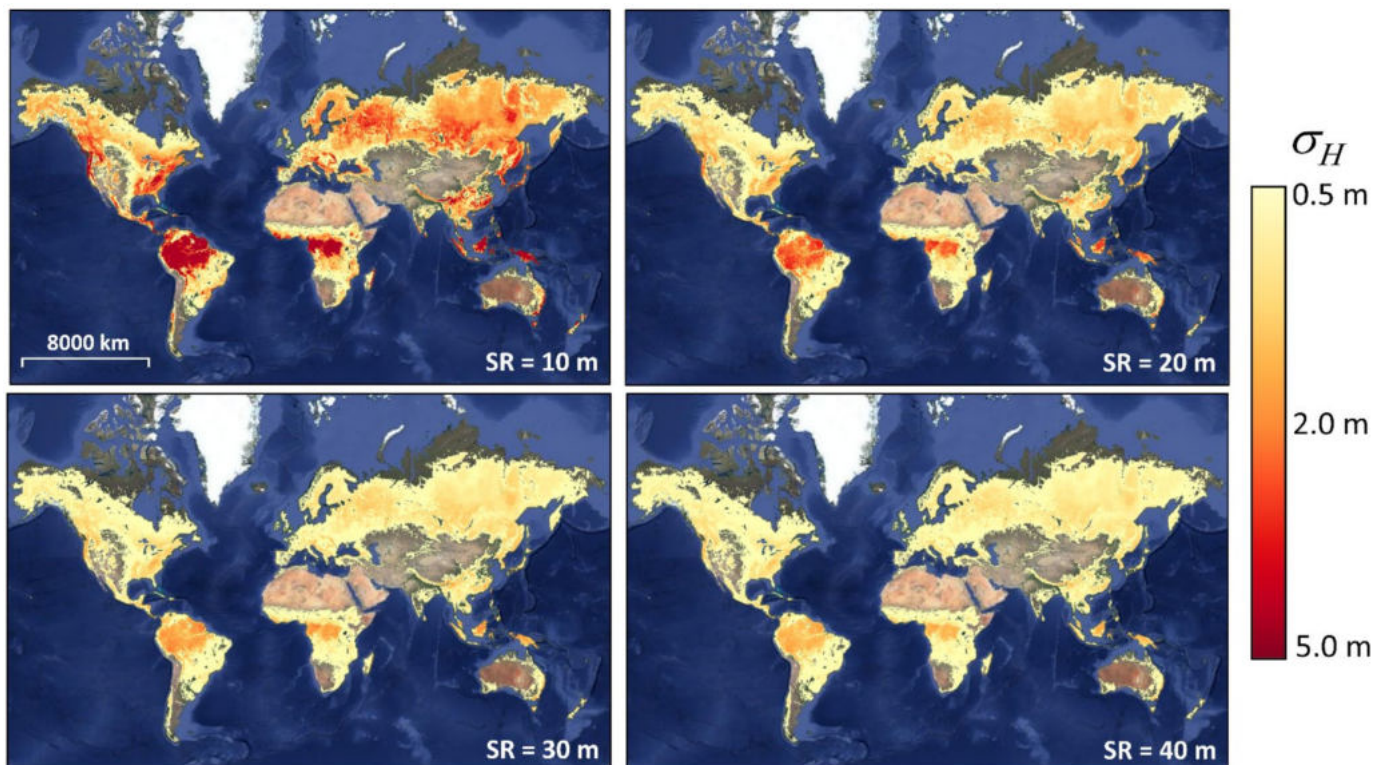
Figure 8. $\sigma_H(x, y)$ maps at global scale computed in GEE. Four operative scenarios were proposed by assuming *SR* at 10m, 20 m, 30 m, 40 m respectively.
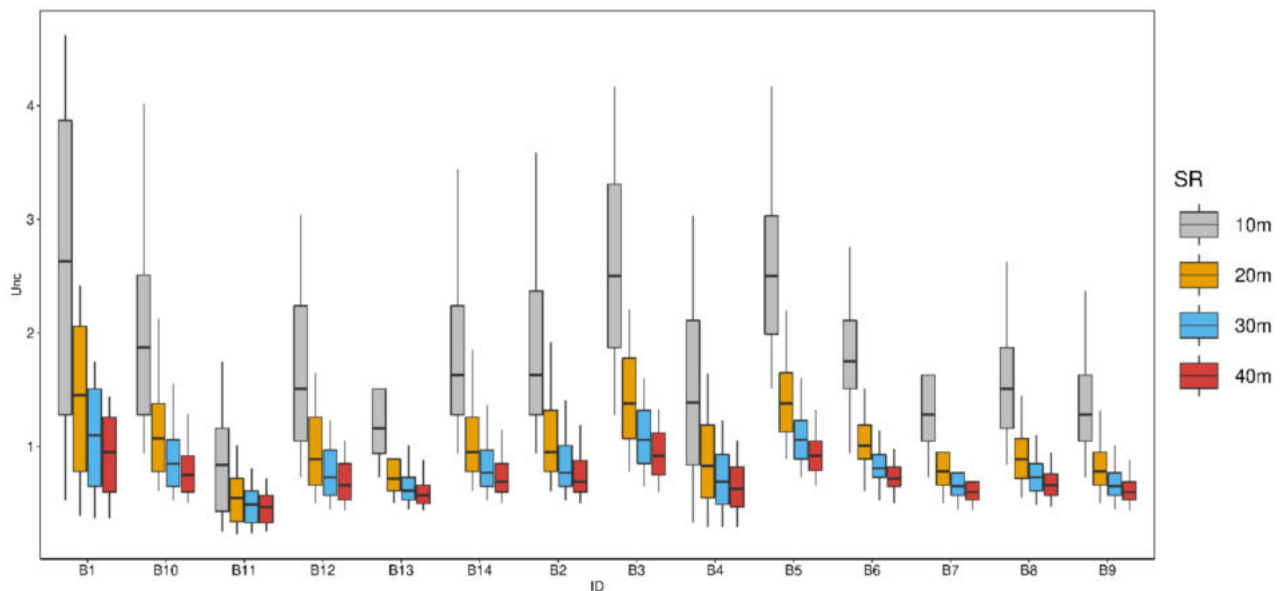
Figure 9. $\sigma_H(x, y)$ values distribution for forest biomes according to four operative scenarios.

In general, as already observed globally in Figure 8, σ_H decreases as *SR* increases in all investigated biomes. The highest σ_H are also observed at *SR* = 10m, while the lowest values at *SR* = 40 m. In particular, the average value of σ_H result to be equal to 1.83 m, 1.05 m, 0.83 m, and 0.73 m for *SR* equal to 10, 20, 30, and 40 m, respectively. Specifically, σ_H for different biomes included in this work the following observations can be carried out: (i) Tundra (B11), desert-xeric shrublands (B13), and tropical-subtropical-savannas and shrublands (B7) are the biomes with the lowest σ_H (all scenarios average was found equal to 0.60, 0.85, 0.92 m respectively); (ii) Tropical and subtropical moist broadleaf

forest (B1), Tropical and subtropical coniferous (B3), and temperate conifer forests (B5) are the biomes with the highest σ_H (all scenarios average was found equal to 1.50, 1.52, and 1.54 m, respectively). In this context, the results obtained are consistent with the theoretical assessment proposed in this work and recent literature. In particular, it is well known that different vegetation, and consequently different biomes, can certainly affect tree height estimation. However, the main factors that can affect σ_H can be traced back to forest structure, tree height, terrain topography, tree species, and tree lean [26,43]. For example, regarding biome B11, represented by Tundra and therefore characterized by small vegetation, low values of σ_H were found. Conversely, considering biome B1, represented by tropical and subtropical broadleaf forests and therefore characterized by very tall trees, high values of σ_H were found. These results are consistent to the ones reported by Hyyppa [51], Hush [48], and Korning [49]. The first one investigated forest height estimation and pointed out that the accuracy of tree height measurement decreases as vegetation height increases (especially with trees > 25 m). The second and third one highlight that deciduous trees show lower tree height accuracy.

A further consideration that can be deduced in Figure 9 is the dispersion of σ_H in the different *SR* classes. σ_H distribution result to be more heterogenous in the class of *SR* = 10 m (σ_H ranges between 2 m and 4 m), while it results to be homogenous when *SR* increases (around one meter). Consequently, it can be defined that within the same biome the measurement of vegetation height is affected by SR. This result is supported by Skovsgaard [6], who confirms that distance from the measured trees can affected the tree high estimation. Indeed, for some biomes the variation of *SR* has a considerable impact on σ_H values. For example, concerning Taiga (B6) at *SR* = 10 m, the σ_H values are very different from those at *SR* = 20 m. This behaviour generally occurs between *SR* equal to 10 and 20 m and takes place in other biomes as B13, B14, B3, B5, B8, and B9. Conversely, in other biomes this phenomenon is less present. For example, in B1, B11, and B4, boxplots at *SR* = 10 m and 20 m are similar only for 50–60% of the time, therefore in this cases *SR* variation seems to less affect the final σ_H value. Regarding the transition of *SR* between 30 m and 40 m, the differences in terms of σ_H seem to disappear or even become irrelevant in many cases.

This finding can be interpreted as an absence of σ_H decrease as *SR* increases in some contexts for specific biomes. Consequently, from an operational point of view, these findings could be extremely useful for increasing the speed of surveys (avoiding too be far away from the target) and simultaneously maintaining precise tree height estimates. For example, in Tundra and Shrublands biomes, low σ_H values were found for all *SR* scenarios. Another interesting outcome concerning these biomes is the following: comparing these accuracies to the expected vegetation height in such biomes, they highlight how hypsometer is not the proper instrument for height surveys in shrublands and Tundra since the uncertainty is higher than expected vegetation height. In such biomes other instruments such as a graduated pole or tape measure can guarantee a rapid and more accurate measure of small vegetation height than the ones retrieved by hypsometer.

Finally, it is worth to remind that provided world-wide estimates of height uncertainty are "optimistic" since they are based on theoretical conditions. In real operative conditions, other unpredictable factors such as apex visibility/identification and stem curvature (e.g., in coppices) could negatively affects the height accuracy.

4. Conclusions

In this work, a statistically based operative method for estimating tree height measurement uncertainty (σ_H) was proposed using the variance propagation law. The aim was to model the behaviour of σ_H in different operative context. Therefore, several simulations were performed involving factors such as tree height, survey distances, and terrain slope. Regarding the terrain slope, results shown that this parameter poorly affect σ_H.

Concerning the first two parameters, results proved that σ_H could greatly be affected by *H* and *SR* resulting in a tree height error between 0.5 m and up to 20 m (worst case).

Moreover, in this work a simple rule of thumb was proposed (*H-SR* ratio equal to 1:2) to minimize height uncertainty under 5% of H.

Concerning the sensitivity analysis of all parameters involved in the σ_H, results shows that the w_α and w_θ were the more relevant (their sum is about 95%), while $w_{corr\,(SR,\alpha)}$, $w_{corr(SR,\theta)}$, w_φ, and w_{SR} contribution result to be very low in σ_H determination (under 1%).

Finally, to give a practical example of such deductions, tree height uncertainty was mapped at the global scale using Google Earth Engine and summarized per forest biomes. Results proved that tropical biomes have higher uncertainty (from 1 m to 4 m) while shrublands and tundra the lowest (under 1 m). The proposed approach proved to be an operative tool useful both in forest research and forest management context. It allows to better consider the uncertainty of forest estimates, alerting the user about the significance of difference that one could test between forest stands or between the same stand at different times.

References

1. Segura, M.; Kanninen, M. Allometric Models for Tree Volume and Total Aboveground Biomass in a Tropical Humid Forest in Costa Rica. *Biotropica J. Biol. Conserv.* **2005**, *37*, 2–8. [CrossRef]
2. Laurin, G.V.; Ding, J.; Disney, M.; Bartholomeus, H.; Herold, M.; Papale, D.; Valentini, R. Tree Height in Tropical Forest as Measured by Different Ground, Proximal, and Remote Sensing Instruments, and Impacts on above Ground Biomass Estimates. *Int. J. Appl. Earth Obs. Geoinf.* **2019**, *82*, 101899.
3. Hao, Z.; Zhang, J.; Song, B.; Ye, J.; Li, B. Vertical Structure and Spatial Associations of Dominant Tree Species in an Old-Growth Temperate Forest. *For. Ecol. Manag.* **2007**, *252*, 1–11. [CrossRef]
4. Song, B.; Chen, J.; Desander, P.V.; Reed, D.D.; Bradshaw, G.A.; Franklin, J.F. Modeling Canopy Structure and Heterogeneity across Scales: From Crowns to Canopy. *For. Ecol. Manag.* **1997**, *96*, 217–229. [CrossRef]
5. Spies, T.A. Forest Structure: A Key to the Ecosystem. *Northwest Sci.* **1998**, *72*, 34–36.
6. Skovsgaard, J.P.; Johannsen, V.K.; Vanclay, J.K. Accuracy and Precision of Two Laser Dendrometers. *For. Int. J. For. Res.* **1998**, *71*, 131–139. [CrossRef]
7. Ochal, W.; Socha, J.; Pierzchalski, M. The Effect of the Calculation Method, Plot Size, and Stand Density on the Accuracy of Top Height Estimation in Norway Spruce Stands. *Iforest-Biogeosciences For.* **2017**, *10*, 498. [CrossRef]
8. Momo, E.J.; De Petris, S.; Sarvia, F.; Borgogno-Mondino, E. Addressing Management Practices of Private Forests by Remote Sensing and Open Data: A Tentative Procedure. *Remote Sens. Appl. Soc. Environ.* **2021**, *23*, 100563. [CrossRef]
9. Lund, H.G. When Is a Forest Not a Forest? *J. For.* **2002**, *100*, 21–28.
10. Sillett, S.C.; Van Pelt, R.; Koch, G.W.; Ambrose, A.R.; Carroll, A.L.; Antoine, M.E.; Mifsud, B.M. Increasing Wood Production through Old Age in Tall Trees. *For. Ecol. Manag.* **2010**, *259*, 976–994. [CrossRef]
11. Hanewinkel, M.; Hummel, S.; Albrecht, A. Assessing Natural Hazards in Forestry for Risk Management: A Review. *Eur. J. For. Res.* **2011**, *130*, 329–351. [CrossRef]
12. Martins, A.C.; Willig, M.R.; Presley, S.J.; Marinho-Filho, J. Effects of Forest Height and Vertical Complexity on Abundance and Biodiversity of Bats in Amazonia. *For. Ecol. Manag.* **2017**, *391*, 427–435. [CrossRef]
13. Bohn, F.J.; Huth, A. The Importance of Forest Structure to Biodiversity–Productivity Relationships. *R. Soc. Open Sci.* **2017**, *4*, 160521. [CrossRef] [PubMed]
14. Purves, D.W.; Lichstein, J.W.; Strigul, N.; Pacala, S.W. Predicting and Understanding Forest Dynamics Using a Simple Tractable Model. *Proc. Natl. Acad. Sci. USA* **2008**, *105*, 17018–17022. [CrossRef]
15. Pan, Y.; Birdsey, R.A.; Fang, J.; Houghton, R.; Kauppi, P.E.; Kurz, W.A.; Phillips, O.L.; Shvidenko, A.; Lewis, S.L.; Canadell, J.G. A Large and Persistent Carbon Sink in the World's Forests. *Science* **2011**, *333*, 988–993. [CrossRef] [PubMed]

16. Tavoni, M.; Sohngen, B.; Bosetti, V. Forestry and the Carbon Market Response to Stabilize Climate. *Energy Policy* **2007**, *35*, 5346–5353. [CrossRef]
17. Ter-Mikaelian, M.T.; Korzukhin, M.D. Biomass Equations for Sixty-Five North American Tree Species. *For. Ecol. Manag.* **1997**, *97*, 1–24. [CrossRef]
18. Zianis, D.; Muukkonen, P.; Mäkipää, R.; Mencuccini, M. *Biomass and Stem Volume Equations for Tree Species in Europe*; The Finnish Society of Forest Science: Helsinki, Finland, 2005.
19. Neumann, M.; Moreno, A.; Mues, V.; Härkönen, S.; Mura, M.; Bouriaud, O.; Lang, M.; Achten, W.M.; Thivolle-Cazat, A.; Bronisz, K. Comparison of Carbon Estimation Methods for European Forests. *For. Ecol. Manag.* **2016**, *361*, 397–420. [CrossRef]
20. De Petris, S.; Sarvia, F.; Borgogno-Mondino, E. RPAS-Based Photogrammetry to Support Tree Stability Assessment: Longing for Precision Arboriculture. *Urban For. Urban Green.* **2020**, *55*, 126862. [CrossRef]
21. De Petris, S.; Berretti, R.; Sarvia, F.; Borgogno Mondino, E. When a Definition Makes the Difference: Operative Issues about Tree Height Measures from RPAS-Derived CHMs. *iForest-Biogeosci. For.* **2020**, *13*, 404. [CrossRef]
22. Yin, D.; Wang, L. How to Assess the Accuracy of the Individual Tree-Based Forest Inventory Derived from Remotely Sensed Data: A Review. *Int. J. Remote Sens.* **2016**, *37*, 4521–4553. [CrossRef]
23. West, P.W.; West, P.W. *Tree and Forest Measurement*; Springer: Cham, Switzerland, 2009.
24. van Laar, A.; Akça, A. *Forest Mensuration (Managing Forest Ecosystems)*, 2nd ed.; Completely Rev. and Supplemented; Springer: Dordrecht, The Netherlands, 2007; ISBN 978-1-4020-5990-2.
25. Larsen, D.R.; Hann, D.W.; Stearns-Smith, S.C. Accuracy and Precision of the Tangent Method of Measuring Tree Height. *West. J. Appl. For.* **1987**, *2*, 26–28. [CrossRef]
26. Stereńczak, K.; Mielcarek, M.; Wertz, B.; Bronisz, K.; Zajączkowski, G.; Jagodziński, A.M.; Ochał, W.; Skorupski, M. Factors Influencing the Accuracy of Ground-Based Tree-Height Measurements for Major European Tree Species. *J. Environ. Manag.* **2019**, *231*, 1284–1292. [CrossRef]
27. Köhl, M.; Magnussen, S.S.; Marchetti, M. *Sampling Methods, Remote Sensing and GIS Multiresource Forest Inventory*; Springer Science & Business Media: Berlin/Heidelberg, Germany, 2006.
28. Vogt, J.M.; Fischer, B.C. A Protocol for Citizen Science Monitoring of Recently-Planted Urban Trees. In *Urban Forests, Ecosystem Services and Management*; Blum, J., Ed.; Apple Academic Press: New York, NY, USA, 2017; pp. 153–186.
29. Mascaro, J.; Detto, M.; Asner, G.P.; Muller-Landau, H.C. Evaluating Uncertainty in Mapping Forest Carbon with Airborne LiDAR. *Remote Sens. Environ.* **2011**, *115*, 3770–3774. [CrossRef]
30. Clark, N.A.; Wynne, R.H.; Schmoldt, D.L. A Review of Past Research on Dendrometers. *For. Sci.* **2000**, *46*, 570–576.
31. Pariyar, S.; Mandal, R.A. Comparative Tree Height Measurement Using Different Instrument. *Int. J. Ecol. Environ. Sci.* **2019**, *1*, 12–17.
32. Williams, M.S.; Bechtold, W.A.; LaBau, V.J. Five Instruments for Measuring Tree Height: An Evaluation. *South. J. Appl. For.* **1994**, *18*, 76–82. [CrossRef]
33. Wing, M.G.; Solmie, D.; Kellogg, L. Comparing Digital Range Finders for Forestry Applications. *J. For.* **2004**, *102*, 16–20.
34. Saliu, I.S.; Satyanarayana, B.; Fisol, M.A.B.; Wolswijk, G.; Decannière, C.; Lucas, R.; Otero, V.; Dahdouh-Guebas, F. An Accuracy Analysis of Mangrove Tree Height Mensuration Using Forestry Techniques, Hypsometers and UAVs. *Estuarine Coast. Shelf Sci.* **2021**, *248*, 106971. [CrossRef]
35. Vasilescu, M.M. Standard Error of Tree Height Using Vertex III. *Bull. Transilv. Univ. Brasov. For. Wood Ind. Agric. Food Eng. Ser. II* **2013**, *6*, 75.
36. Schreuder, H.T.; Gregoire, T.G.; Wood, G.B. *Sampling Methods for Multiresource Forest Inventory*; John Wiley & Sons: New York, NY, USA, 1993.
37. Ku, H.H. Notes on the Use of Propagation of Error Formulas. *J. Res. Natl. Bur. Stand.* **1966**, *70*, 263–273. [CrossRef]
38. Laser Technology Inc TruPulse 200 User's Manual 2018. Available online: https://lasertech.com/wp-content/uploads/LTI-TruPulse-200.6.pdf (accessed on 5 June 2022).
39. Simard, M.; Pinto, N.; Fisher, J.B.; Baccini, A. Mapping Forest Canopy Height Globally with Spaceborne Lidar. *J. Geophys. Res. Biogeosciences* **2011**, *116*. [CrossRef]
40. Hayashi, M.; Saigusa, N.; Oguma, H.; Yamagata, Y. Forest Canopy Height Estimation Using ICESat/GLAS Data and Error Factor Analysis in Hokkaido, Japan. *ISPRS J. Photogramm. Remote Sens.* **2013**, *81*, 12–18. [CrossRef]
41. Hastings, D.A.; Dunbar, P. Development & Assessment of the Global Land One-Km Base Elevation Digital Elevation Model (GLOBE). *Group* **1998**, *4*, 218–221.
42. Dinerstein, E.; Olson, D.; Joshi, A.; Vynne, C.; Burgess, N.D.; Wikramanayake, E.; Hahn, N.; Palminteri, S.; Hedao, P.; Noss, R. An Ecoregion-Based Approach to Protecting Half the Terrestrial Realm. *BioScience* **2017**, *67*, 534–545. [CrossRef] [PubMed]
43. Ojoatre, S.; Zhang, C.; Hussin, Y.A.; Kloosterman, H.E.; Ismail, M.H. Assessing the Uncertainty of Tree Height and Aboveground Biomass from Terrestrial Laser Scanner and Hypsometer Using Airborne LiDAR Data in Tropical Rainforests. *IEEE J. Sel. Top. Appl. Earth Obs. Remote Sens.* **2019**, *12*, 4149–4159. [CrossRef]
44. Lira, I. *Evaluating the Measurement Uncertainty: Fundamentals and Practical Guidance*; CRC Press: Boca Raton, FL, USA, 2002.
45. Muelaner, J.E.; Wang, Z.; Jamshidi, J.; Maropoulos, P.G.; Mileham, A.R.; Hughes, E.B.; Forbes, A.B. Study of the Uncertainty of Angle Measurement for a Rotary-Laser Automatic Theodolite (R-LAT). *Proc. Inst. Mech. Eng. Part B J. Eng. Manuf.* **2009**, *223*, 217–229. [CrossRef]

46. Gorelick, N.; Hancher, M.; Dixon, M.; Ilyushchenko, S.; Thau, D.; Moore, R. Google Earth Engine: Planetary-Scale Geospatial Analysis for Everyone. *Remote Sens. Environ.* **2017**, *202*, 18–27. [CrossRef]

47. Bragg, D.C. *The Sine Method as a More Accurate Height Predictor for Hardwoods*; e-Gen. Tech. Rep. SRS–101; U.S. Department of Agriculture, Forest Service, Southern Research Station: 23-33. [CD-ROM]; U.S. Department of Agriculture: Washington, DC, USA, 2007.

48. Husch, B.; Beers, T.W.; Kershaw, J.A., Jr. *Forest Mensuration*; John Wiley & Sons: Hoboken, NJ, USA, 2002.

49. Korning, J.; Thomsen, K. A New Method for Measuring Tree Height in Tropical Rain Forest. *J. Veg. Sci.* **1994**, *5*, 139–140. [CrossRef]

50. Božić, M.; Čavlović, J.; Lukić, N.; Teslak, K.; Kos, D. Efficiency of Ultrasonic Vertex III Hypsometer Compared to the Most Commonly Used Hypsometers in Croatian Forestry. *Croat. J. For. Eng. J. Theory Appl. For. Eng.* **2005**, *26*, 91–99.

51. Hyyppä, J.; Pyysalo, U.; Hyyppä, H.; Samberg, A. Elevation Accuracy of Laser Scanning-Derived Digital Terrain and Target Models in Forest Environment. In Proceedings of the Proceedings of EARSeL-SIG-Workshop LIDAR, Dresden, Germany, 23–26 October 2016; pp. 16–17.